CHEMICAL ENGINEERING TRANSACTIONS
VOL. 103, 2023
A publication of AIDIC
The Italian Association of Chemical Engineering
Online at www.cetjournal.it
Guest Editors: Petar S. Varbanov, Panos Seferlis, Yee Van Fan, Athanasios Papadopoulos

ISBN 979-12-81206-02-1; **ISSN** 2283-9216
DOI: 10.3303/CET23103139

Bandgap Tailoring of ZnO Using Metallic Sulphides for Enhanced Visible-light-active Photocatalytic Water Treatment

Rachel Mugumo*, Emmanuel O. Ichipi, Shepherd M. Tichapondwa, Evans M. N. Chirwa

Water Utilisation and Environmental Engineering Division, Department of Chemical Engineering, University of Pretoria, Pretoria 0028, South Africa
rachelmugumo@gmail.com

The combination of a wide bandgap Zinc oxide (ZnO ~3.4 eV) semiconductor photocatalyst with typical metallic sulphides, namely, silver sulphide (Ag_2S), ferric sulphide (FeS) and nickel sulphide (NiS), all of a similar narrow bandgap (~0.90 eV), resulted in the red-shifting of photocatalytic activity towards the visible-light region. In this work, Ag_2S/ZnO, FeS/ZnO and NiS/ZnO nanocomposites were synthesised via a facile combustion method. The physicochemical properties of the synthesised nanocomposites were characterised using X-ray diffractometer (XRD), scanning electron microscopy (SEM), and Ultraviolet diffuse reflectance spectroscopy (UV-vis DRS) techniques. Data obtained from the UV-vis DRS results were interpolated to estimate the bandgap energy of each nanocomposite using Tauc plots. The bandgap energy of ZnO was tailored from 3.30 eV to 2.15 eV, 1.91 eV and 1.85 eV for Ag_2S/ZnO, FeS/ZnO and NiS/ZnO. The photocatalytic efficiency of the as-synthesised nanocomposites at was investigated on the removal of 10 mgL^{-1} of methylene blue (MB) dye at 1 gL^{-1} catalyst loading. Results showed that Ag_2S/ZnO, FeS/ZnO and NiS/ZnO achieved the removal of 99 %, 88 % and 81 % of MB dye after 120 min and a complete removal after 150 min of simulated visible light irradiation. The slope of the linear regression curve was calculated and found to follow a pseudo-first-order reaction kinetics with R^2 values higher than 0.96. Finally, the results obtained from this study point to a way forward in the concept of bandgap engineering in photocatalysis as well as the efficient treatment method of dye-polluted effluent from the textile industry.

1. Introduction

The world's fast-growing development in technology has led to vast industrial production of daily-used products with a wide range of applications (Fouda et al., 2020). Dyes, among these products, are crucial in the fashion, textile, pharmaceuticals, leather, plastic, ink and paper industries, with approximately 280,000 t/y synthetic dyes discharged into the environment (Waghchaure et al., 2022). These organic pigments, which are stable and non-biodegradable, are hazardous to the environment, aquatic life and human health as they cause mutagenic, carcinogenic and genotoxic disorders (Shakoor and Nasar, 2017). The dye's presence in water influences the photocatalytic process as sunlight penetration declines, negatively affecting aquatic flora-fauna (Waghchaure et al., 2022).

Physicochemical methods such as ion exchange, coagulation, membrane filtration, adsorption and chemical oxidation have been explored (Munawar et al., 2020). However, the maintenance costs and operational costs are very high. Hence the drive towards green, cost-effective alternative promising techniques such as photocatalysis must be investigated (Fouda et al., 2020). Heterogeneous photocatalysis technology is deemed effective in the eradication of contaminants from wastewater under visible light irradiation, which promotes the application of various semiconductor metal oxides as photocatalysts. The applicability of metal oxides as photocatalysts is influenced by the characteristic intrinsic properties such as the light absorption range, morphology, particle size, specific surface area and electronic band structure (Puneetha et al., 2021). Bandgap engineering is a principal aspect in the designing, fabricating and tuning of semiconductor photocatalysts' optical properties to achieve desired applications (Samavati et al., 2021). During photon irradiation, light absorption

Paper Received: 17 April 2023; Revised: 28 July 2023; Accepted: 27 August 2023
Please cite this article as: Mugumo R., Ichipi E.O., Tichapondwa S.M., Chirwa E.M.N., 2023, Bandgap Tailoring of ZnO Using Metallic Sulphides for Enhanced Visible-light-active Photocatalytic Water Treatment, Chemical Engineering Transactions, 103, 829-834 DOI:10.3303/CET23103139

initially occurs at specific wavelengths resulting in electron excitation from the valence band (V_B) to the conduction band (C_B). this excitation phenomenon and enables various energy conversions promoting the semiconductor photocatalytic activity (Puneetha et al., 2021).
Zinc oxide (ZnO) has been widely researched as an excellent photocatalytic material and a suitable substitute for TiO_2 since they possess similar properties. Among various metal oxide semiconductors, ZnO has wide applicability in optoelectronics, spintronics and photonics due to its excellent physical properties (Zhang and Xu, 2020). Wurtize ZnO is an intrinsic n-type semiconductor with a direct and wide bandgap energy of 3.44 eV at low temperatures and 3.37 eV at room temperature. It has a superiorly large exciton binding energy of ~ 60 meV, high chemical stability and high redox potential (Shokri et al., 2020). ZnO bandgap modification is significantly vital in the adjustment of optical and electronic properties, which involves attenuated materials size reduction. For instance, changing from bulk to compact alters the bandgap. This can be further attuned by varying ZnO film thickness (Samavati et al., 2021). Shokri et al. (2020) reported an outstandingly reduced bandgap of about 0.7 eV in the binary nanocomposite compared to pristine ZnO. Puneetha et al. (2021) synthesised ZnO and ZnO/GO nanocomposites using a simple co-precipitation method and reported a lowered bandgap energy value of approximately 2.71 eV in ZnO/GO compared to the bare ZnO. Zhang and Xu (2020) developed the Gaussian process regression (GPR) model to elucidate the statistical relationship among grain size, lattice parameters and bandgap energy for doped-ZnO which was reported to be about 2.10 eV. The above studies vividly illustrate an improved photodegradation efficacy in the reduced band-gaped semiconductor photocatalyst.
To the best of our knowledge, this study reports for the first time a comparative study of metallic sulphide doped ZnO, which share a similar narrow bandgap of about 0.90 eV. The prepared ZnO, Ag_2S/ZnO, FeS/ZnO and NiS/ZnO nanocomposites were synthesised using an adopted innovative facile environmentally friendly thermal decomposition method and investigated their photodegradation performance in methylene blue (MB) dye pollutant removal under visible light irradiation. It is demonstrated that the sulphur-based/ZnO heterostructures had lowered bandgap energies leading to the exhibition of excellent photocatalytic performance under visible light irradiation.

2. Experimental

2.1 Materials

Silver (II) nitrate hexahydrate [$Ag(NO_3)_2.6H_2O$] (silver precursor) and zinc oxide [ZnO] were purchased from Glassworld (Johannesburg, South Africa). Ferric (III) nitrate nonahydrate [$Fe_2(NO_3)_3.9H_2O$] (iron precursor) and thiourea [$(NH_2)_2CS$] (sulphur precursor and oxidant fuel) were purchased from Sigma-Aldrich (St Louis, MO, United States). Nickel (II) nitrate hexahydrate [$Ni(NO_3)_2.6H_2O$] (nickel precursor) purchased from Merck (Darmstadt, Germany). Methylene blue dye (the model organic pollutant) was purchased from Sigma-Aldrich (Johannesburg, South Africa). All reagents were used without further purification. Deionised water (DI) was used as a solvent throughout this study.

2.2 Synthesis

Ag_2S/ZnO, FeS/ZnO and NiS/ZnO nanomaterials were synthesised using a solid phase one-pot combustion synthesis method. ZnO, $Ag(NO_3)_2.6H_2O$, and $(NH_2)_2CS$ were measured and weighed in a 2:1:0.25 ratio. The weighted mixture was initially added to a clean crucible before thoroughly mixing it and then calcined at 400 °C for 30 min. The obtained product was ground to a powdery catalyst using pastel and mortar. NiS/ZnO was prepared using zinc oxide, nickel (II) nitrate hexahydrate and thiourea, and FeS/ZnO using zinc oxide, ferric (III) nitrate nonahydrate and thiourea following the same method of synthesis. This fabrication method was adopted from the experimental procedure previously reported by Mugumo et al. (2022).

2.3 Characterisation

The prepared XRD samples were analysed using the PANalytical X'Pert Pro powder diffractometer in θ–θ configuration with an X'Celerator detector and variable divergence- and fixed receiving slits with Fe filtered Co-Kα radiation (λ=1.789Å). The crystallinity of the sample was determined through the selection of the best–fitting pattern from the ICSD database to the measured diffraction pattern, using X'Pert Highscore plus software. The materials SEM images were captured on a Zeiss Ultra PLUS FEG SEM and the optical absorption spectra of the synthesised nanomaterials were measured using a Hitachi U-3900 single monochromatic double-beam system that uses UV-solutions software program.

2.4 Photocatalytic activity

The photocatalytic performance of the synthesised composites (Ag_2S/ZnO, NiS/ZnO and FeS/ZnO) was investigated by conducting the degradation of methylene blue dye diluted in deionised water under visible light

irradiation. The experimental set-up consisted of a wooden box unit with a cubic size measuring (92 × 70 × 70) cm^3 fitted with three fluorescent day lamps (18 W each) which were used as the visible light irradiation source. The photodegradation tests were conducted by loading 10 gL^{-1} of the respective photocatalyst into 100 mL of 10 ppm methylene blue dye solution. The suspension was stirred for 30 min in the dark to allow for adsorption-desorption equilibrium prior to 2 h of visible light irradiation. Aliquots samples of 2 ml were extracted every half m for centrifugation at 9,000 rpm for 10 min. The collected solution was filtered using 0.45 µm Millipore microfilters, and the filtrate samples were measured at a wavelength of 663 nm using a Labotec UV/Vis Lightwave II spectrophotometer. The obtained degradation efficacy was determined using Eq(1) below.

$$\%\ Degradation = \frac{(C_0 - C_t)}{C_0} \times 100 \quad (1)$$

where C_o is the initial MB dye concentration and Ct is MB dye concentration at time, t.

3. Results and discussion

3.1 X-ray Diffraction analysis

The phase structures of the synthesised crystalline nanomaterials (ZnO, Ag_2S/ZnO, FeS/ZnO and NiS/ZnO) were determined using the XRD analysis and are depicted in Figure 1. The XRD patterns of all the synthesised samples precisely match with the ZnO structure (JCPDS No. 36 – 1451) which indicates the purity of the synthesised desired products. The sharp and intense peaks of pristine ZnO with 2θ values of 37.1°, 40.2°, 42.3°, 55.8°, 66.8°, 74.5° and 80.9° corresponding to the crystal planes (100), (002), (101), (102), (110), (103) and (112), are in good agreement with the hexagonal wurtzite structure of ZnO and further shows the high crystallinity and purity of the crystals (Ichipi et al., 2022). The additional peak in each transitional metal sulphur-based nanomaterial spectra confirms the presence of the respective metal sulphide (Ag2S, FeS and NiS). It can be postulated that the negligible difference in metallic sulphur-based/ZnO XRD spectra is due to the synthesis ratio of 1:4. As a result, little detection of the metal-sulphide semiconductors as small amounts were used in the synthesis of the binary nanocomposites.

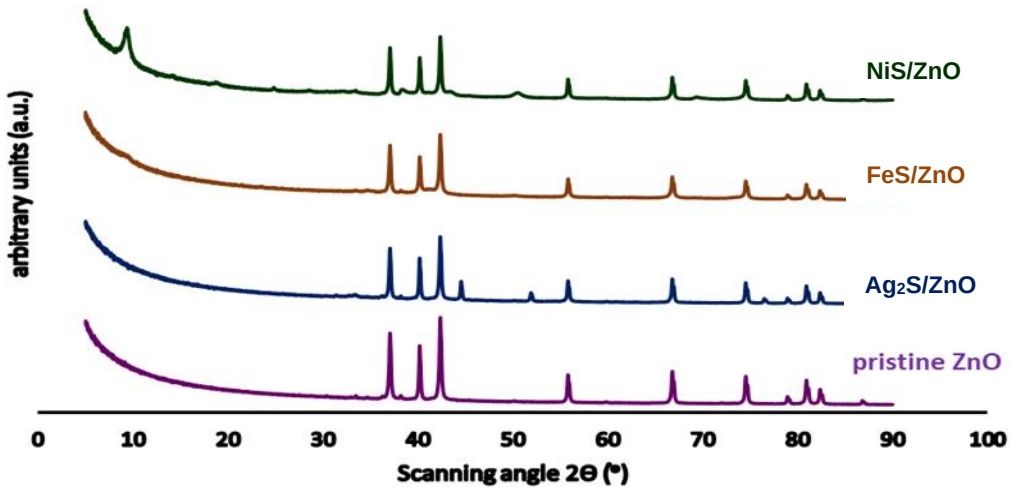

Figure 1: XRD spectra for ZnO, Ag_2S/ZnO, FeS/ZnO and NiS/ZnO composites

3.2 SEM analysis

The morphology of the synthesised materials (Ag_2S/ZnO, FeS/ZnO and NiS/ZnO) was studied using the SEM analysis technique. Figure 2 depict the nanomaterials SEM images as clusters and agglomerate mixtures with angular, spherical, and cubic-like structures. Aggregations result from the interaction between the metal sulphides and ZnO in reaction conditions during the annealing process at high temperatures. The aggregation process also directly influences the homogeneity of the distribution of nanoparticles (Alshamsi et al., 2021).

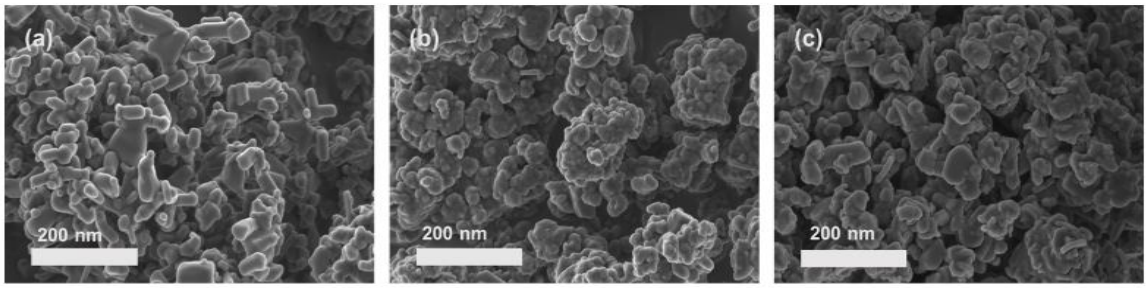

Figure 2: SEM image of synthesised (a) Ag_2S/ZnO, (b) FeS/ZnO and (c) NiS/ZnO

3.3 Optical bandgap analysis

A diffuse reflectance UV-vis spectrum (UV-DRS) was used in the examination of the optical and photon-absorption properties of the synthesised materials. The absorption edges were found in the range of 320 – 380 nm. The bandgap energy of the nanomaterials was measured from the UV-DRS data using Eq(2):

$$(\alpha hv)^{\frac{1}{n}} = (hv - E_g) \quad (2)$$

where α, v and h denote molar absorption coefficient, frequency, and the Plank's constant, while E_g denotes the bandgap energy. The 'n' value can either be 0.5 or 2 depending on its direct or indirect transitions.
As shown in Figure 3, the bandgap is obtained by plotting $(\alpha hv)^2$ against hc and extrapolation of the tangent intercept on the x-axis. The determined bandgap energy of pristine ZnO ~ 3.30 eV whilst a redshift is noted in the metallic sulphur-based/ZnO nanocomposites reporting reduced bandgap energy values of 2.15 eV, 1.91 eV and 1.85 eV for Ag_2S/ZnO, FeS/ZnO and NiS/ZnO. The photo absorption properties of the semiconductors are directly related to their energy band structure which exhibit significantly enhanced properties. For instance, a narrow bandgap suggests high photocatalytic activity (Alshamsi et al., 2021).

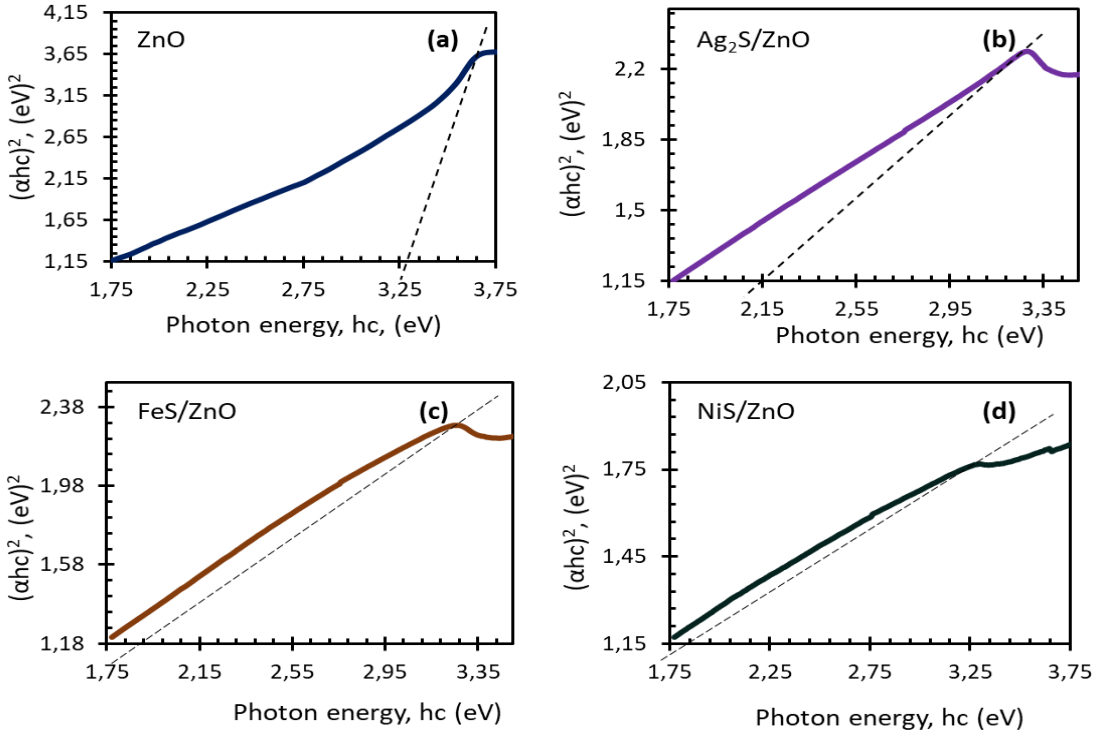

Figure 3: Tauc plots of the estimated bandgap energy of (a) ZnO, (b) Ag_2S/ZnO, (c) FeS/ZnO and (d) NiS/ZnO nanocomposites

4. Degradation studies

The photocatalytic performance of the synthesised metallic sulphur-based/ZnO (Ag_2S/ZnO, FeS/ZnO and NiS/ZnO) photocatalysts was investigated for comparison in the degradation of methylene blue dye under visible light irradiation as illustrated in Figure 4(a). Control experiments were first performed under visible light irradiation to investigate the influence of light only (photolysis) and resulted in negligible MB dye degradation. Subsequently, the photodegradation tests were performed using the as-synthesised nanocomposites at 1 gL^{-1} catalyst loading in 10 mgL^{-1} MB dye solution for 120 min under visible light irradiation. The degradation percentage was calculated using Eq(1). The reactor was allowed to stir for an initial 30 min in the dark to establish an adsorption-desorption equilibrium before exposure to visible light irradiation for a further 120 min. As shown in Figure 4 below, Ag_2S/ZnO, FeS/ZnO and NiS/ZnO photocatalysts achieved outstanding MB dye removal of 99 %, 88 % and 81 %. The Ag_2S/ZnO nanocomposites yielded the highest MB dye removal, followed by FeS/ZnO and the NiS/ZnO photocatalyst achieved the least degradation. This excellently enhanced photocatalytic efficiency of the binary nanocomposites can be attributed to the reduced bandgap energies (Alshamsi et al., 2021). Additionally, to further compare the photodegradation efficacy of the synthesised catalysts, the pseudo-first-order maximum reaction kinetic constants were quantitively employed and reported R^2 values higher than 0.96. Figure 4(b) clearly depicts k_{max} values following a trend Ag_2S/ZnO > FeS/ZnO > NiS/ZnO, which supports the obtained photocatalytic activity of each synthesised nanomaterials as shown in Figure 4(a).

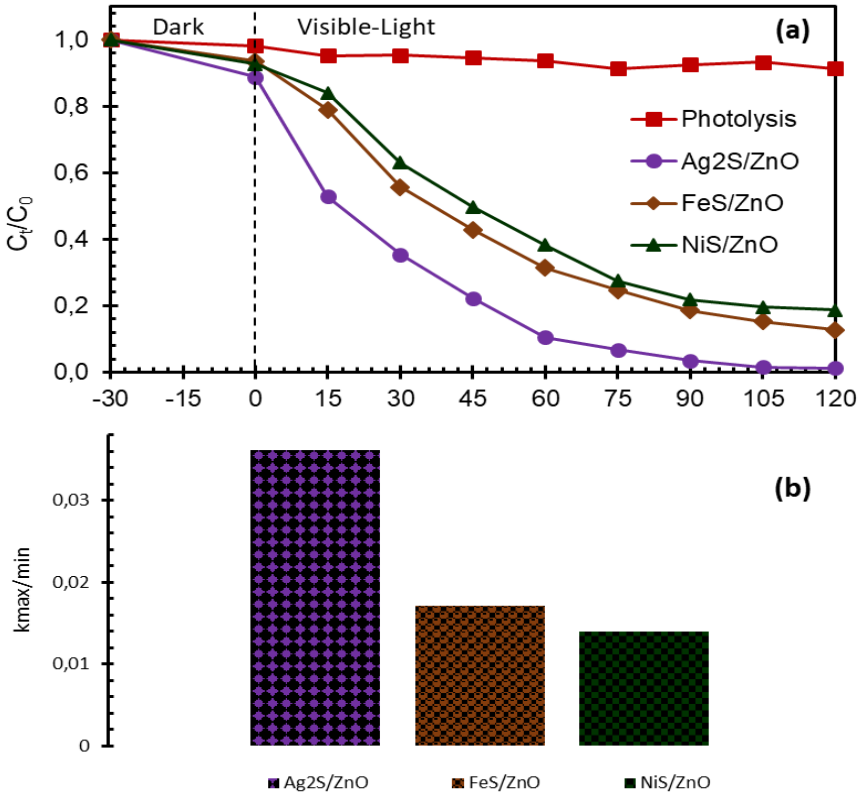

Figure 4: (a) Nanocomposites performance in methylene blue dye photodegradation under visible light irradiation and (b) pseudo-first-order maximum reaction kinetic constant values for each synthesised catalyst

5. Conclusions

In the present study, ZnO and the metallic sulphide-based/ZnO (Ag_2S/ZnO, FeS/ZnO and NiS/ZnO) nanocomposites were successfully prepared by a facile thermal decomposition method. Various characterisation techniques were employed to ascertain the synthesised nanomaterials morphology, purity, crystallinity and absorption potential. The Tauc plot estimation results reveal the successful narrowing of ZnO bandgap when the metal sulphide semiconductors were incorporated. The metallic sulphide-based/ZnO nanocomposites exhibited enhanced photocatalytic performance which indicates efficient charge separation and strong visible light harvesting characteristics. Among all the synthesised nanocomposites, the binary

Ag_2S/ZnO achieved the highest photodegradation performance with 99 % methylene blue dye removal in 120 min under visible light irradiation. The pseudo-first-order maximum reaction kinetic constants follow the same trend as the obtained photodegradation activity with R^2 values higher than 0.96. The attained results prompt further research into bandgap tailoring of semiconductor photocatalysts for improved photocatalytic activity.

Acknowledgements

This work is based on research financially supported by the National Research Fund (NRF) of South Africa (Grant numbers: EQP180503325881, TTK18024324064) and Rand Water Chair in Water Utilisation (RW01413/18) awarded to Prof. Evans M.N. Chirwa and Prof. Shepherd M. Tichapondwa.

References

Alshamsi H.A., Beshkar F., Amiri O., Salavati-Niasari M., 2021, Porous hollow Ag/Ag_2S/Ag_3PO_4 nanocomposites as highly efficient heterojunction photocatalysts for the removal of antibiotics under simulated sunlight irradiation, Chemosphere, 274**,** 129765.

Fouda A., Salem S.S., Wassel A.R., Hamza M.F., Shaheen T.I., 2020, Optimization of green biosynthesized visible light active CuO/ZnO nano-photocatalysts for the degradation of organic methylene blue dye. Heliyon, 6**,** e04896.

Ichipi E.O., Tichapondwa S.M., Chirwa E.M., 2022, Plasmonic effect and bandgap tailoring of Ag/Ag_2S doped on ZnO nanocomposites for enhanced visible-light photocatalysis, Advanced Powder Technology, 33**,** 103596.

Mugumo R., Tichapondwa S.M., Chirwa E.M., 2022, Effects of Initial pH and CuS/ZnS Loading in Rhodamine B Photodegradation Under Visible Light Irradiation, Chemical Engineering Transactions, 94**,** 1027-1032.

Munawar T., Yasmeen S., Mukhtar F., Nadeem M.S., Mahmood K., Saif M.S., Hasan M., Ali A., Hussain F., Iqbal F., 2020, ZnO.9CeO.05MO.05O (M= Er, Y, V) nanocrystals: structural and energy bandgap engineering of ZnO for enhancing photocatalytic and antibacterial activity, Ceramics International*,* 46**,** 14369-14383.

Puneetha J., Kottam N., Rathna A., 2021, Investigation of photocatalytic degradation of crystal violet and its correlation with bandgap in ZnO and ZnO/GO nanohybrid, Inorganic Chemistry Communications, 125**,** 108460.

Samavati A., Awang A., Samavati Z., Ismail A.F., Othman M., Velashjerdi M., Rostami A., 2021, Influence of ZnO nanostructure configuration on tailoring the optical bandgap: Theory and experiment, Materials Science and Engineering: B, 263**,** 114811.

Shakoor S., Nasar A., 2017, Adsorptive treatment of hazardous methylene blue dye from artificially contaminated water using cucumis sativus peel waste as a low-cost adsorbent, Groundwater for Sustainable Development, 5**,** 152-159.

Shokri A., Yazdani A., Rahimi K., 2020, Possible bandgap values of graphene-like ZnO in density functional theory corrected by the Hubbard U term and HSE hybrid functional, Materials Today Communications, 22**,** 100756.

Waghchaure R.H., Adole V.A., Jagdale B.S., 2022, Photocatalytic degradation of methylene blue, rhodamine B, methyl orange and Eriochrome black T dyes by modified ZnO nanocatalysts: A concise review, Inorganic Chemistry Communications**,** 109764.

Zhang Y., Xu X., 2020, Machine learning optical band gaps of doped-ZnO films, Optik, 217**,** 164808.